Investigation of carbon transport by $^{13}CH_4$ injection through graphite and tungsten test limiters in TEXTOR

A Kreter[1], D Borodin[1], S Brezinsek[1], S Droste[1], T Hirai[2], A Kirschner[1], A Litnovsky[1], M Mayer[3], V Philipps[1], A Pospieszczyk[1], Y Sakawa[4], U Samm[1], O Schmitz[1], G Sergienko[1], T Tanabe[4], Y Ueda[5], P Wienhold[1] and TEXTOR team

[1] Institut für Plasmaphysik, Forschungszentrum Jülich, Association EURATOM-FZJ, Trilateral Euregio Cluster, Germany (www.fz-juelich.de/ipp)
[2] Institut für Werkstoffe und Verfahren der Energietechnik, Forschungszentrum Jülich, Association EURATOM-FZJ, Germany (www.fz-juelich.de/iwv)
[3] Max-Planck-Institut für Plasmaphysik, EURATOM Association, Garching, Germany
[4] Department of Energy Engineering and Science, Nagoya University, Nagoya 464-8603, Japan
[5] Graduate School of Engineering, Osaka University, Osaka 565-0871, Japan

E-mail: a.kreter@fz-juelich.de

Abstract. $^{13}CH_4$ was injected through graphite and tungsten spherical limiters in reproducible TEXTOR discharges. These materials were chosen, as they represent the actual compromise for the plasma facing components in the ITER divertor. ^{13}C was used in order to distinguish injected and intrinsic carbon in the layer deposited on the limiter surface. Shot-by-shot video recordings show a continuous growth of the deposit near the injection hole. A pronounced difference in the ^{13}C deposition pattern on the graphite and tungsten limiters was observed. *Post-mortem* surface analysis showed that the ratios of the locally deposited to the injected amount of carbon are 4 % for graphite and 0.3 % for tungsten. The margins of the carbon layer deposited on tungsten are significantly steeper in comparison to the graphite limiter case. The large difference in the ^{13}C deposition efficiency can be explained by direct reflection of carbon from tungsten and enhanced sputtering of carbon on tungsten substrate. Nucleation is suggested to be an important mechanism for carbon deposition on tungsten. Monte Carlo impurity transport calculations by the ERO code reproduce reasonably the experimental results for the graphite limiter.

PACS numbers: 52.40.Hf, 52.55.Fa, 52.65.Pp, 82.80.Ch, 82.80.Ms, 82.80.Yc

1. Introduction

The material choice for the plasma facing components (PFCs) in the next-step fusion device ITER is one of the most crucial questions for a sustainable and safe operation at high power loads. At present, a mix of materials with beryllium at the main chamber wall, tungsten and carbon fiber composite (CFC) in the divertor region is foreseen [1]. Carbon based materials have outstanding thermal properties, such as high thermal conductivity and lack of melting, and therefore are widely used in present generation fusion devices. However, carbon is subject to relatively high physical sputtering by background plasma particles. Moreover, chemical erosion by formation of hydrocarbon molecules like CD_4 leads to even higher carbon erosion rate. Some fraction of eroded carbon atoms, which is not locally re-deposited, can be transported along plasma wetted surfaces as well as to shadowed regions. The use of carbon based materials in a fusion reactor is restricted by the problem of tritium retention in the re-deposited carbon layers. Consequently, for ITER carbon PFCs are foreseen only for the strike point areas. However, carbon still can be transported from there and re-deposited in the neighbouring divertor regions covered by tungsten, affecting the overall balance of co-deposited tritium. Moreover, carbon migration can cause mixed material effects and influence the performance of the tungsten PFCs.

The aim of the experiments presented here was to investigate the local carbon transport for the materials according to the ITER divertor PFC choice. The experimental results were compared with calculations by the ERO code, a modelling tool to describe the material transport and

erosion/deposition processes of PFCs [2]. The experiment followed the $^{13}CH_4$ injection studies started at TEXTOR in 1997 [3].
Section 2 describes the experiments at TEXTOR. The experimental set-up, the discharge scenario including plasma parameters as well as spectroscopy data are presented. Post-mortem surface analysis is the subject of section 3. Section 4 deals with the ERO code modelling for the graphite limiter. In section 5 the results are summarized. Possible mechanisms explaining the differences in the results for the graphite and tungsten limiters are discussed.

2. Experiment description

TEXTOR is a medium size tokamak (major radius $R_0 = 1.75$ m, minor radius $a = 0.46$ m defined by the toroidal belt ALT-II limiter) with circular plasma cross-section. Test limiters were inserted in the TEXTOR vacuum vessel using the limiter lock system at the bottom of the machine [4] (figure 1). Spherical limiters with a size of 120 mm in toroidal direction and 80 mm in poloidal direction and a curvature radius of 70 mm were used in the experiments (figure 2). The limiters were pre-heated to 400-450°C and positioned in the scrape-off layer (SOL) at $r = 0.48$ m, 20 mm outside the last closed flux surface (LCFS). The injection hole was situated at the ion drift side 15 mm away from the tip of the limiter, so that the radial position of the opening was 1.7 mm behind the limiter tip. The diameter of the injection hole was 2 mm for the graphite limiter and 1 mm for the tungsten one. The limiter ion drift side is exposed to particle and heat fluxes in SOL typically by a factor of about five higher than the electron drift side. This results from the difference in connection lengths towards the ALT-II limiter (22 m for the ion drift side and 4 m for the electron drift side) at the position of the limiter lock system.
$^{13}CH_4$ injection rates of up to $\sim 10^{19}$ s^{-1} were similar for both limiters despite the difference in hole diameters. The total amount of injected $^{13}CH_4$ ($5.5 \cdot 10^{20}$ molecules for the graphite and $5.7 \cdot 10^{20}$ for the tungsten limiter) was almost identical.
The tungsten limiter was exposed to eight reproducible NBI heated plasma discharges, the graphite limiter for six discharges with NBI and two Ohmic discharges. The discharges were performed at a toroidal magnetic field of $B_t = 2.25$ T and a plasma current of $I_P = 350$ kA with a central line-integrated electron density of $\bar{n}_{e0} = 3.5 \cdot 10^{19}$ m^{-3}. The scenario of a typical NBI heated discharge for the graphite limiter is shown in figure 3. Plasma parameters in the tungsten limiter experiment were similar.
$^{13}CH_4$ was used as a trace impurity. No influence of the gas injection on the measured plasma parameters and on the carbon concentration in the plasma was observed. This was also confirmed by the analysis of a collecting probe exposed to the SOL plasma at the other side of the torus during the experiment. The carbon layer deposited on this probe had a ^{13}C fraction of only 2-3 %.
Measurements of edge plasma profiles by the thermal helium beam diagnostic positioned at the low field side of the torus confirm a good reproducibility of the discharges within one experimental series as well as for both series (figure 4). Electron densities and temperatures at LCFS were in the range of $n_e^{LCFS} = (1.4\text{-}1.6) \cdot 10^{19}$ m^{-3} and $T_e^{LCFS} = 35\text{-}40$ eV, respectively. At the position of the limiter tip they decayed to $n_e^{LIM} = (1.5\text{-}2.0) \cdot 10^{18}$ m^{-3} and $T_e^{LIM} = 20\text{-}25$ eV, respectively.
The $^{13}CH_4$ injection may still have had an effect on the local plasma parameters near the injection hole, which were not measured. However, as the injection rates were similar for both limiters, the local alteration of the plasma parameters should be the same. Therefore, the experimental conditions can be excluded from the interpretation of possible deviations in the results for both limiters.
Spectroscopic measurements were done using horizontal and vertical observation systems [5]. The horizontal observation system was equipped with a video camera to measure two-dimensional spectral line intensity distributions of C III (465 nm) or CH+CD (431 nm). A similar video system with a H_α (656 nm) interference filter was applied for the vertical observation. The growth of deposited layers can be observed by the reduction of the reflected light intensity from the limiter. Figure 5 shows the shot-by-shot evolution of the carbon deposit on the tungsten limiter surface during the discharge series with $^{13}CH_4$ injection recorded by the vertical system. One observes a continuous expansion of the deposition pattern in the vicinity of the injection hole. The deposition at the limiter ion drift side (upper edge of the limiter images) showed also continuous growth, as can be seen from the reduced reflection of the light from the ALT-II limiter blades.

3. Post-mortem limiter analysis

A pronounced difference in the ^{13}C deposition pattern on the limiter surfaces can already be seen by a visual inspection (figure 6). The layer of amorphous co-deposited carbon and hydrogen (a-C:H layer) on tungsten shows well defined margins with steep edges surrounded by a shiny net-erosion zone, whereas the deposit on graphite has a larger area with a smoother profile and blurred margins. On the graphite limiter, there is also no clear separation between the layers deposited by the injection and by the background carbon flux, as in the case of the tungsten limiter. The oblong shape of the deposits can be attributed to the preferred direction of the local ^{13}C transport defined by direction of the SOL plasma flow parallel to the magnetic field combined with the E×B force, as indicated in figure 6. Thereby E is the radial electric field.

The limiter surfaces were investigated post-mortem by the interference fringe analysis, secondary ion mass spectrometry (SIMS) and nuclear reaction analysis (NRA). The interference fringe analysis allows for the determination of the total carbon amount in the deposited film. The sputter SIMS technique delivers depth profiles of different elements and isotopes. The isotopic ratio $^{13}C/^{12}C$ can also be determined by SIMS. The absolute amounts of ^{13}C, ^{12}C and D can be measured by NRA, but without depth resolution. A combination of these surface analysis techniques allows us to determine integral amounts of deposited elements and their distributions. Figure 7 shows as an example of NRA measurements the two-dimensional distribution of the sum of ^{13}C and ^{12}C on the tungsten substrate.

One of the characteristics, which can be used for a direct comparison of the experiments and modelling, is the ^{13}C deposition efficiency. We define the ^{13}C deposition efficiency as the ratio of the amount of ^{13}C in the deposit near the hole to the injected amount of ^{13}C. The surface areas taken into account for the efficiency determination are indicated in figure 6 for both limiters. The ^{13}C amounts deposited in these areas are $2 \cdot 10^{19}$ atoms for the graphite limiter and $1.5 \cdot 10^{18}$ atoms for the tungsten one. Correspondingly, the ^{13}C deposition efficiencies differ by about one order of magnitude (4 % for graphite and 0.3 % for tungsten).

The maximum of the deposition is situated near the injection hole for both limiters (figure 8). The distributions of ^{13}C and D are strongly peaked near the hole, whereas ^{12}C is distributed more uniformly. The maximum layer thickness is only about a factor of 2 larger for the graphite (2.1 μm) than for the tungsten (1.1 μm) limiter. Therefore, the large difference in the ^{13}C deposition efficiency is mainly due to the difference in the area of deposition on both limiters. The ratio of ^{13}C to total C obtained by NRA and SIMS varies from more than 90 % in the vicinity of the injection hole to 30-40 % at the deposit edge for both experiments. The D-to-C ratio is in the range of 10-20 % for graphite and 5-15 % for tungsten.

To characterize the steepness of the deposit edges their thickness profiles were fitted by an exponential function. The characteristic decay lengths of the deposit thickness for the graphite limiter were 4 mm to 6 mm with higher values for the edge in the preferred direction of the local ^{13}C transport. The values for the tungsten limiter at the positions shown in figure 7 vary between 0.7 mm and 3.1 mm. Note the significantly sharper edges for the tungsten case. Here, again, longer decay lengths were observed for the edge in the preferred carbon transport direction. For the opposite direction a remarkably short decay length of 0.7 mm was derived.

4. ERO code modelling for the graphite limiter

Modelling by the ERO code was performed for the graphite limiter experiments. The modelling for the tungsten limiter case is not presented here, because the surface interlayer model currently implemented in the ERO code is not suitable to accurately simulate the dynamic processes in mixed carbon-tungsten layers. An effort to implement a more sophisticated TriDyn based surface model in the ERO code [6] to simulate mixed materials effects is under way.

The best match with the measured ^{13}C deposition efficiency was found for the assumptions of an effective sticking of zero for hydrocarbon species and an enhanced chemical re-erosion of freshly deposited a-C:H layers (15 % vs. 1.5 % for graphite), resulting in a ^{13}C deposition efficiency of about 10 %. Similar assumptions were also necessary to reproduce the results of the previous $^{13}CH_4$ injection experiment at TEXTOR [7]. The good agreement in the carbon deposition pattern (figure 9) supports the assumptions of low effective sticking of hydrocarbons.

A fair agreement between experiment and modelling was also found for the light emission distributions of both C III and the sum of CH and CD lines (figure 10). The deviations between experiment and modelling result probably from uncertainties in the local plasma parameters. The electron temperature and density of the plasma boundary were measured by the helium beam diagnostic not at the test limiter position, but at the low field side. Slight deviations in the vertical and horizontal plasma positioning can lead to significant poloidal asymmetries of plasma profiles. An ERO test run was performed with the assumption of LCFS at a minor radius of 47 cm instead of 46 cm, resulting in good agreement of the light emission patterns (not shown here). This change of the LCFS position led to a value of the ^{13}C deposition efficiency of 7 %, which is closer to the experimental one (4%).

5. Summary and discussion

In the $^{13}CH_4$ injection experiments a large difference in the ^{13}C deposition efficiency was found for the graphite (4 %) and tungsten (0.3 %) limiters. The results were obtained for similar local plasma parameters in both experiments. Therefore, this difference can be clearly attributed to a substrate material influence.

Several substrate effects can be considered as reasons of the difference in the ^{13}C deposition efficiency. One of them is the effect of kinetic reflections of the incident carbon atoms from the limiter surface (*cf.* the EDDY code modelling for the tungsten-carbon twin limiter experiment in TEXTOR [8]). The reflection coefficient for carbon atoms from carbon substrates is low (*e.g.* $R \approx 10^{-4}$ for normal incident angle and an impact energy of C^+ of 50 eV [9]), whereas it is $R \approx 0.6$ for reflection of carbon from tungsten (figure 11a and 11b). It leads to a change in the balance between carbon erosion and deposition causing larger net-erosion zones on the tungsten substrate. The balance switches to net-deposition in the region of high carbon flux near the injection hole. After reaching a certain thickness the a-C:H layer protects the tungsten substrate, so that further incident carbon atoms do not perceive the high-Z substrate under the a-C:H layer. It results in higher growth rates of the deposit thickness in this region (so-called nucleation, figure 11c). The sharp edges of the carbon deposit on the tungsten surface support this hypothesis. The areal expansion of the a-C:H layer is caused by a step-wise transport through repetitive process of erosion of carbon from the layer and its subsequent re-deposition nearby. This additional carbon source influences the local erosion-deposition balance of carbon at the layer edge. The preferred direction of the layer expansion is defined by the combination of the plasma flow in SOL and the E×B force, explaining the smoother shape of the edge in this direction.

Another possible reason for the difference in the ^{13}C deposition efficiency is the enhancement of physical sputtering of carbon deposited on tungsten. The enhanced erosion of light materials on a heavier substrate has been studied in detail for the case of boron on carbon and tungsten [10]. To sputter a deposited atom, the incident plasma particle has to change its momentum direction by a reflection from an underlying atom. Being reflected from heavy tungsten, the plasma particle retains more energy and therefore has a higher probability to sputter a carbon atom. A simplified picture of this process is shown in figure 12. The nucleation effect of the build-up of the protective carbon layer on top of the tungsten substrate is also applicable in this case.

Our present knowledge does not allow us to give a definite answer to the question which of these both effects (kinetic reflections of carbon and enhanced physical sputtering) is more important for affecting the deposition on tungsten. Currently there are experimental and modelling activities [6] going on to explore this issue. The first results of these investigations indicate that it is the combination of both effects which leads to the reduced deposition efficiency for high-Z materials.

Mixed material effects (*e. g.* tungsten carbide formation) can be also considered as a possible reason for the different deposition efficiencies. These mixing processes could lead to less chemical erosion and a lower reflection coefficient [8], enhancing the nucleation effect. However, for our experimental conditions with a relatively low limiter temperature of 400-450°C formation of carbides can be excluded.

The ERO code calculations are in reasonable agreement with the experimental results for the graphite limiter. Low effective sticking for all hydrocarbon species had to be assumed to reproduce the deposition pattern and the value of the deposition efficiency. This assumption is in contrast to

laboratory investigations [11] and observations of the a-C:H layer growth in pump ducts of tokamaks [12, 13], which showed rather high sticking values for at least some hydrocarbon species. In our case the low effective sticking for hydrocarbons can be explained by the self re-erosion of transiently deposited hydrocarbons under the influence of energetic background hydrogen [7].
The difference in the carbon deposition efficiency with lower values for the tungsten substrate than for graphite is favourable for the proposed ITER divertor. In ITER, carbon eroded from the CFC tiles will have a lower probability to stick on the neighbouring divertor surfaces covered by tungsten and build up a-C:H layers on these surfaces. Therefore, the contribution of tungsten covered areas to the overall retention of tritium will remain low and the performance of tungsten PFCs will be less affected. However, the effect of the substrate material on the deposition efficiency may depend on other parameters, *e. g.* local plasma properties and geometry. These questions have to be explored in future investigations, both on the experimental and the modelling sides.

References

[1] Federici G *et al* 2001 *Nucl. Fusion* **41** 1967
[2] Kirschner A *et al* 2000 *Nucl. Fusion* **40** 989
[3] Wienhold P *et al* 2001 *J. Nucl. Mater.* **290-293** 362
[4] Schweer B *et al* 2005 *Fusion Sci. Technol.* **47** 138
[5] Brezinsek S *et al* 2005 *Plasma Phys. Control. Fusion* **47** 615
[6] Droste S *et al* 2006 *Contrib. Plasma Phys.* **46** 628
[7] Kirschner A *et al* 2004 *J. Nucl. Mater.* **328** 62
[8] Ohya K *et al* 2004 *Physica Scripta* **111** 138
[9] Eckstein W 2002 *Calculated Sputtering, Reflection and Range Values* (Max-Planck-Institut für Plasmaphysik Report) **IPP 9/132**
[10] Maier H *et al* 2005 *J. Nucl. Mater.* **337–339** 480
[11] Hopf C *et al* 2000 *J. Appl. Phys.* **87 (6)** 2719
[12] Mayer M *et al* 2003 *J. Nucl. Mater.* **313–316** 429
[13] von Seggern J *et al* 2004 *Physica Scripta* **T111** 118

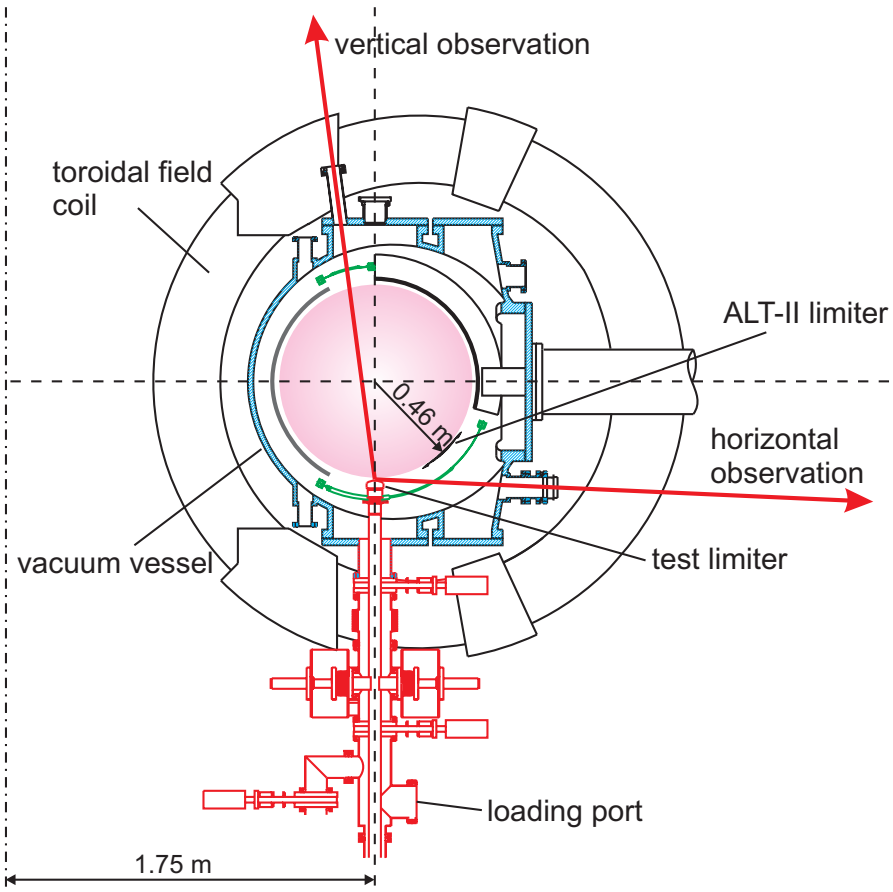

Figure 1. Poloidal cross-section of TEXTOR with the limiter lock system.

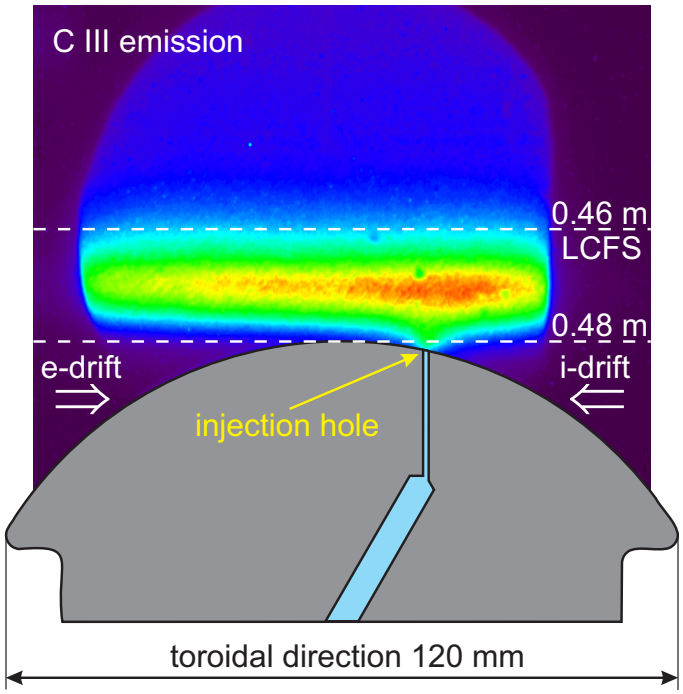

Figure 2. Scheme of the spherical test limiter with injection hole exposed in SOL. CIII light emission during a $^{13}CH_4$ injection through the graphite limiter is shown.

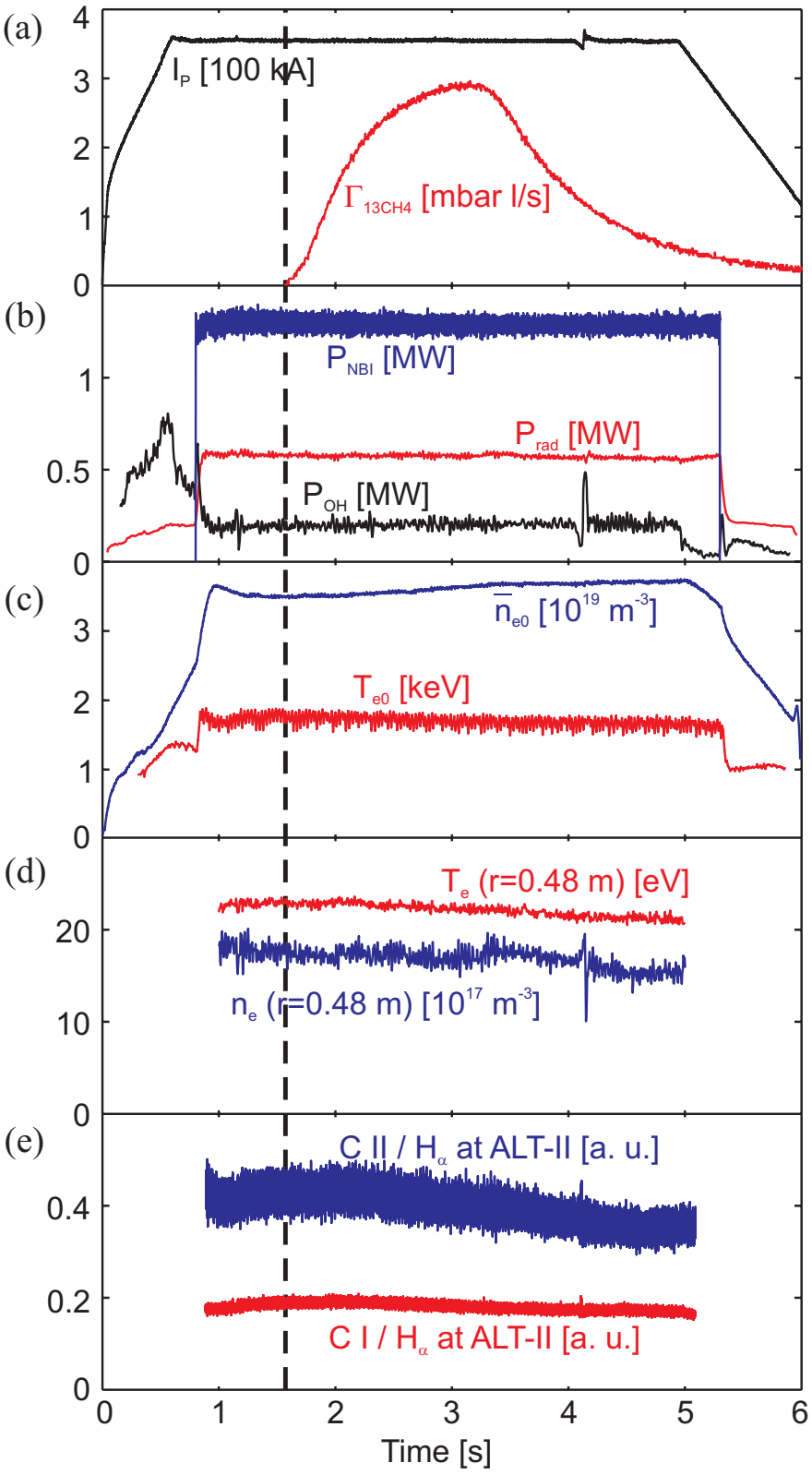

Figure 3. Discharge scenario for the graphite limiter experiment (#95351): (a) plasma current I_P and $^{13}CH_4$ flow rate through the limiter Γ_{13CH4}; (b) neutral beam injection P_{NBI} and Ohmic P_{OH} heating and radiated power P_{rad}; (c) central line averaged electron density $\bar{n}_{e0}$ and central electron temperature T_{e0}; (d) electron density n_e and temperature T_e at r = 0.48 m (limiter tip position); (e) ratios of C I (909.5 nm) and C II (515.4 nm) intensities to H_α measured at the ALT-II limiter. Vertical dashed line indicates the start of the $^{13}CH_4$ injection

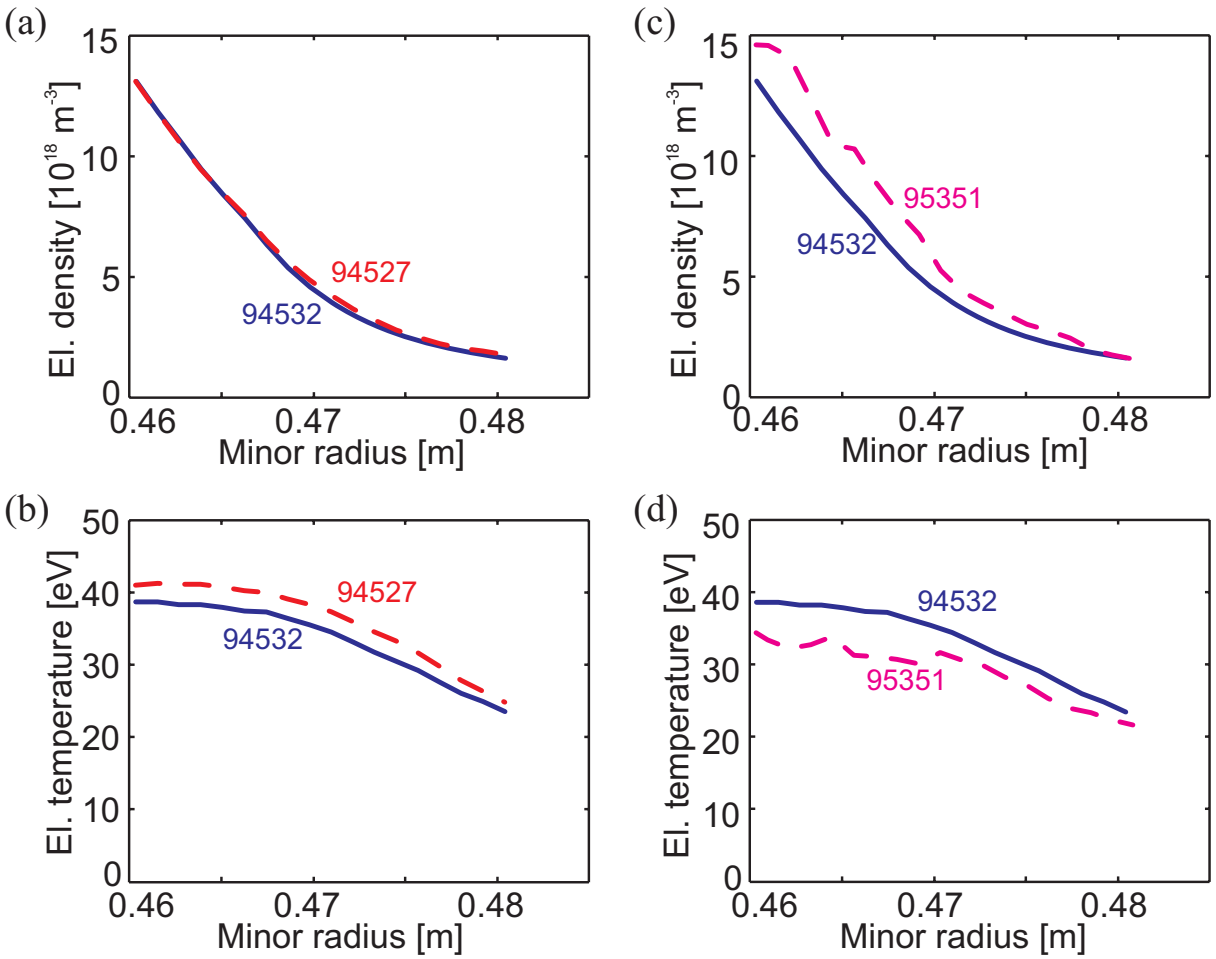

Figure 4. Reproducibility of the SOL profiles of the electron density n_e and temperature T_e: (a) and (b) within one discharge series (#94527 (dashed line) and #94532 (full line) – tungsten limiter experiment); (c) and (d) for two different series (#94532(full line) – tungsten limiter experiment, #95351 (dashed line) – graphite limiter experiment).

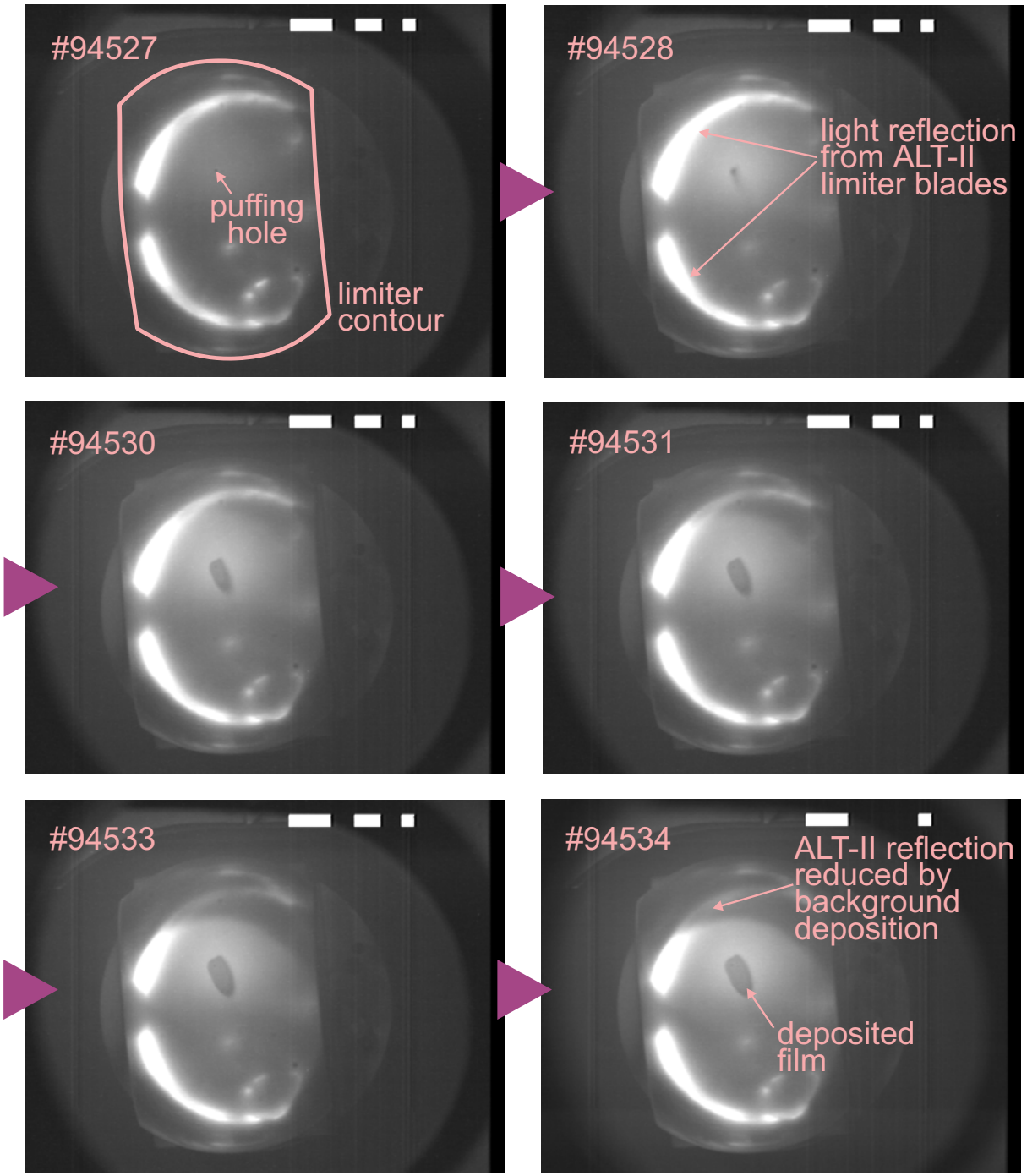

Figure 5. Tungsten limiter vertical view in H_α light: Shot-by-shot evolution of the deposition pattern. The layer originated from the $^{13}CH_4$ injection develops near the injection hole. The light reflection from the ALT-II limiter blades, which is seen as bright curved stripes, is reduced from shot to shot by the background deposition at the ion drift side (upper edge of the limiter images). Images of discharges #94529 and #94532 are not available.

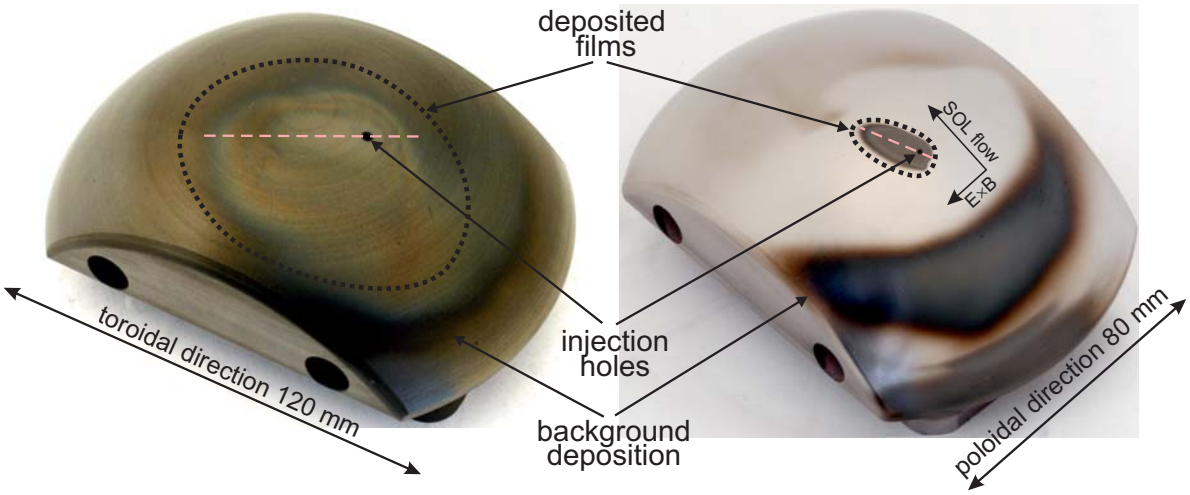

Figure 6. Photographs of the graphite (left) and tungsten (right) limiters after the exposure. Dotted contours indicate the areas where the ^{13}C deposition efficiency was defined. Dashed lines show the position of the NRA measurements presented in figure 8. Directions of the SOL flow and the E×B force are indicated.

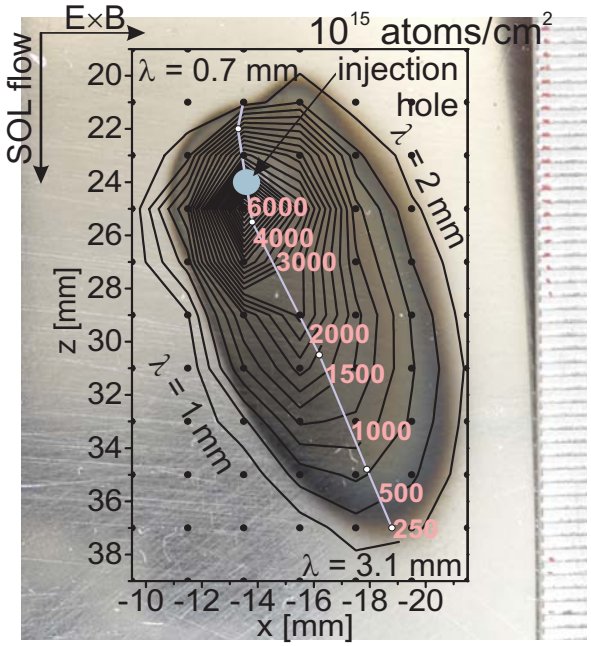

Figure 7. Illustration of the two-dimensional NRA measurements: Contour plot of the measured carbon amount ($^{12}C+^{13}C$, in 10^{15} atoms/cm^2) overlaid on a photograph of the deposit on the tungsten limiter surface. Black dots are NRA measurement points, white dots are additional measurement points for the line scan shown in figure 8. Thickness decay lengths λ for four deposit edges are given.

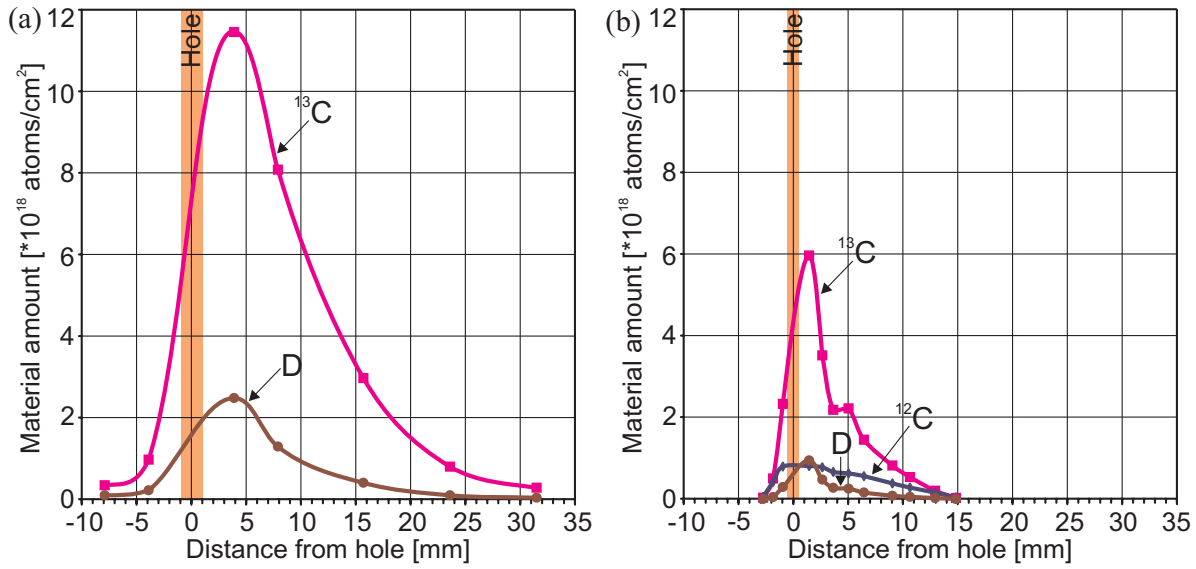

Figure 8. Profiles of deposited materials obtained by NRA for the graphite (a) and tungsten (b) limiters along the lines shown in figure 6. NRA measurement points are indicated and connected by a spline.

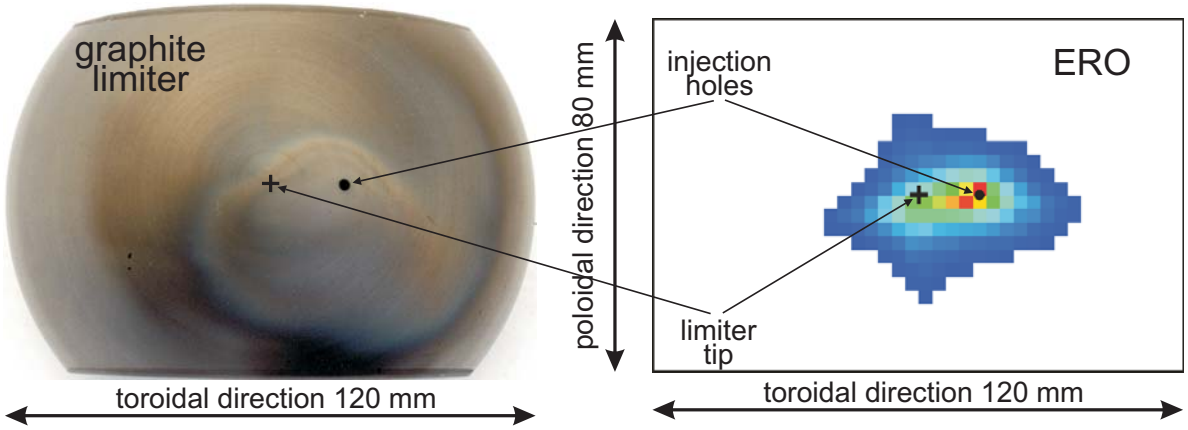

Figure 9. Deposition pattern on the graphite limiter: (left) after exposure in TEXTOR; (right) of ^{13}C calculated by the ERO code.

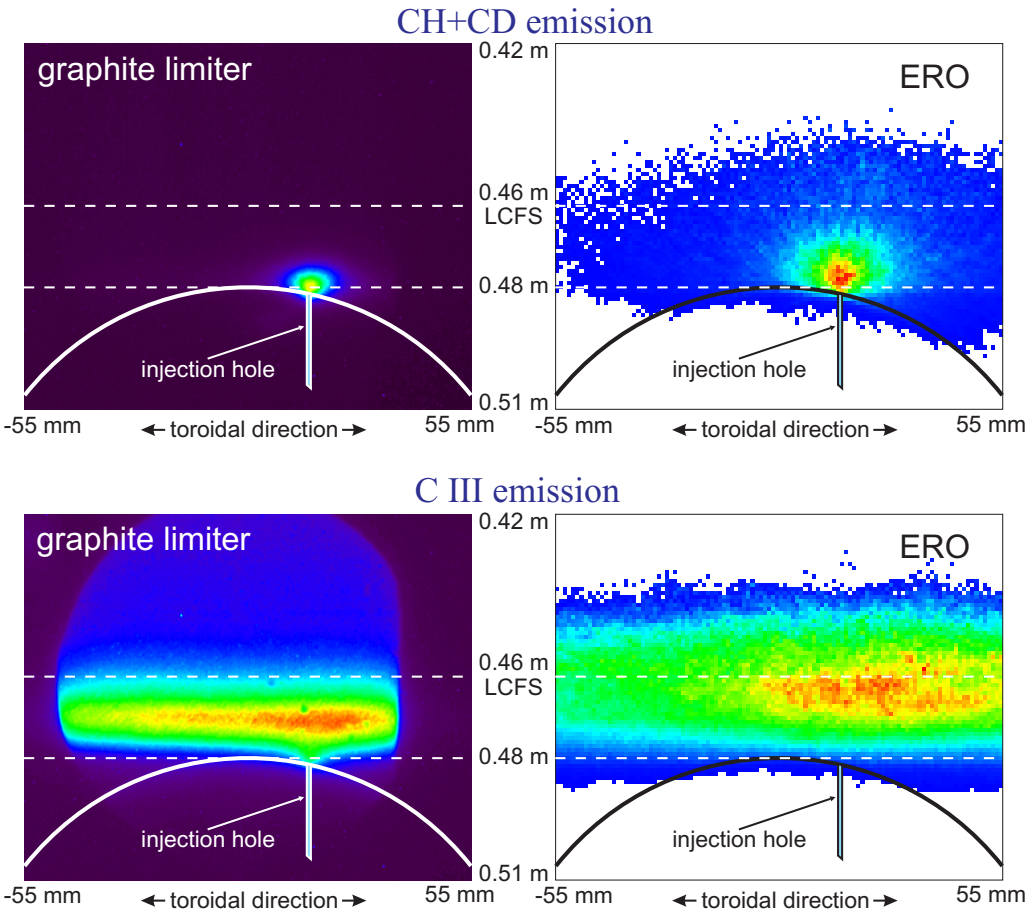

Figure 10. Horizontal view of the sum of CH and CD emission and C III emission measured spectroscopically during a $^{13}CH_4$ injection through the graphite limiter and the corresponding modelling by the ERO code.

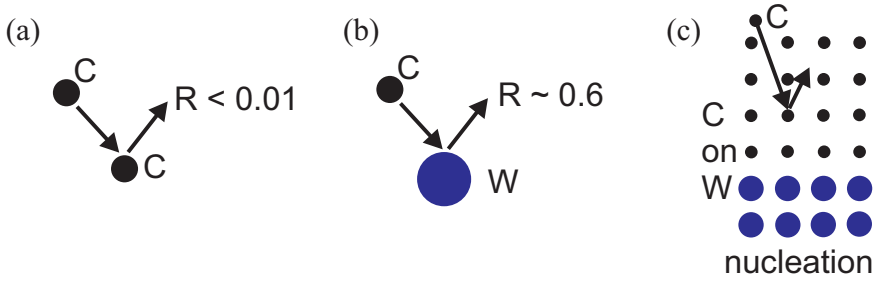

Figure 11. Sketch to illustrate the influence of the reflection of carbon from carbon (a) and from tungsten (b) and the nucleation effect (c).

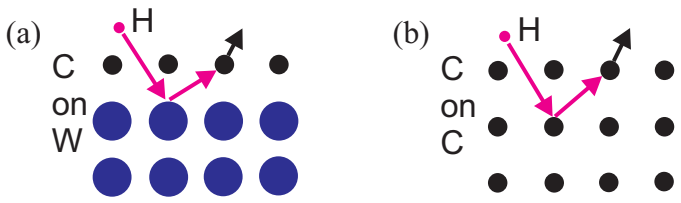

Figure 12. Sketch to illustrate the effect of the sputter enhancement of carbon deposited on tungsten (a) in comparison with carbon deposited on carbon (b).